The Flower Garden Banks *Siderastrea siderea* coral as a candidate Global boundary Stratotype Section and Point for the Anthropocene series

Kristine L DeLong,[1] Kylie Palmer,[1]
Amy J Wagner,[2] Mudith M Weerabaddana,[3]
Niall Slowey,[4] Achim D Herrmann,[1]
Nicolas Duprey,[5] Alfredo Martínez-García,[5]
Jonathan Jung,[5] Irka Hajdas,[6] Neil L Rose,[7]
Sarah L Roberts,[7] Lucy R Roberts,[7] Andrew B Cundy,[8]
Pawel Gaca,[8] J Andrew Milton,[8] Handong Yang,[7]
Simon D Turner,[8] Chun-Yuan Huang,[9]
Chuan-Chou Shen[9] and Jens Zinke[10]

Abstract

The proposed Anthropocene Global Boundary Stratotype Section and Point (GSSP) candidate site of West Flower Garden Bank (27.8762°N, 93.8147°W) is an open ocean location in the Gulf of Mexico with a submerged coral reef and few direct human impacts. Corals contain highly accurate and precise ($<\pm 1$ year) internal chronologies, similar to tree rings, and their exoskeletons are formed of aragonite and can be preserved in the rock record. Here we present results from a large *Siderastrea siderea* coral (core 05WFGB3; 1755–2005 CE) sampled with annual and monthly resolutions that show clear markers of global and regional human impacts. Atmospheric nuclear bomb testing by-products (^{14}C, $^{239+240}Pu$) have clear increases in this coral starting in 1957 for ^{14}C and the first increase in 1956 for $^{239+240}Pu$ (potential bases for the Anthropocene GSSP). Coral $\delta^{13}C$ declined especially after 1956 consistent with the Suess effect resulting from the

[1]Louisiana State University, USA
[2]California State University, USA
[3]University of Arizona, USA
[4]Texas A&M University, College Station, USA
[5]Max Planck Institute for Chemistry (Otto Hahn Institute), Germany
[6]Laboratory of Ion Beam Physics, Switzerland
[7]University College London
[8]University of Southampton, UK

[9]National Taiwan University, ROC
[10]University of Leicester, UK

Corresponding author:
Kristine L DeLong, Department of Geography and Anthropology, Louisiana State University, 227 Howe Russell Geoscience Complex, Baton Rouge, LA 70803-2804, USA.
Email: kdelong@lsu.edu

burning of fossil fuels. Coral skeletal $\delta^{15}N$ starts to increase in 1963 corresponding with the increase in agricultural fertilizers. Coral Hg concentrations (1933–1980) loosely track fluctuations in industrial pollution and coral Ba/Ca increases from 1965–1983 when offshore oil operations expand after 1947. Coral temperature proxies contain the 20th-century global warming trend whereas coral growth declines during this interval.

Introduction

The nuclear age first left its imprint on the Earth in World War II with the detonation of atomic bombs. In the following years, atmospheric nuclear weapons testing was conducted predominately in remote Pacific islands such as Bikini and Eniwetok atolls. Scientists found corals in these atolls contained radioactive bands that correlate to the weapons testing dates and thus one could determine coral growth rates (Knutson et al., 1972). X-ray images (i.e. X-radiographs) of cross-sections cut from coral colonies also reveal high- and low-density bands within the coral skeleton, similar to tree rings, that correlated to radioactive bands and thus years of nuclear testing (Buddemeier et al., 1974; Knutson et al., 1972). Corals are colonial organisms with coral polyps living on top of their aragonite exoskeletons they deposit with varying skeletal density throughout the year as they grow. These annual density bands give scientists time markers for "reading" the environmental history contained in the coral's skeleton, similar to dendrochronology (Lough and Cantin, 2014). The ability to locate individual years in the coral skeleton allows researchers to correlate the coral's skeletal geochemical history to calendar dates with high accuracy. Furthermore, these nuclear weapons testing and the radioactive isotope "bomb spikes," which are present in coral skeletons, have been suggested as the global marker for the Anthropocene Global Boundary Stratotype Section and Point (GSSP) (Waters et al., 2015). The Anthropocene Working Group organized preparatory activities for formalizing the Anthropocene, including events leading to the submission of GSSP proposals, to facilitate a binding decision that the start of the Anthropocene is in the mid-20th century and should align with stratigraphic signals. These activities and proposals are detailed in the introductory article in this special issue (Waters et al., 2023).

This study will examine several radioactive isotopes and other potential Anthropocene markers in detail for a *Siderastrea siderea* coral located in West Flower Garden Bank (WFGB), one of two coral reefs within the Flower Garden Banks National Marine Sanctuary (FGBNMS) in the northern Gulf of Mexico (GoM). The tropical Atlantic coral species *S. siderea* is a particularly good species for archiving the past since it has a relatively slow growth rate (3–6 mm year^{-1}), which means an average-sized coral colony (1–2 m) is older (200–400 years) than faster-growing coral species of the same size and therefore provides longer skeletal records. There is a broad scope of prior geochemical research with *S. siderea*, thus the reason we selected this species for the Anthropocene GSSP candidate; see the review on this species in the Supplemental Material.

The Flower Garden Banks (FGB) are located in the northern GoM at the edge of the wide-continental shelf about 185 km away from the Louisiana and Texas coastline and far from river runoff and coastal upwelling (Figure 1). FGBs' coral reefs are primarily comprised of large boulder-shaped corals and the reefs have ~50% live coral coverage (Schmahl et al., 2008), which is high for Atlantic coral reefs. Furthermore, FGB corals have so far been minimally affected by coral bleaching (Johnston et al., 2019), a condition caused by rising seawater temperatures threatening
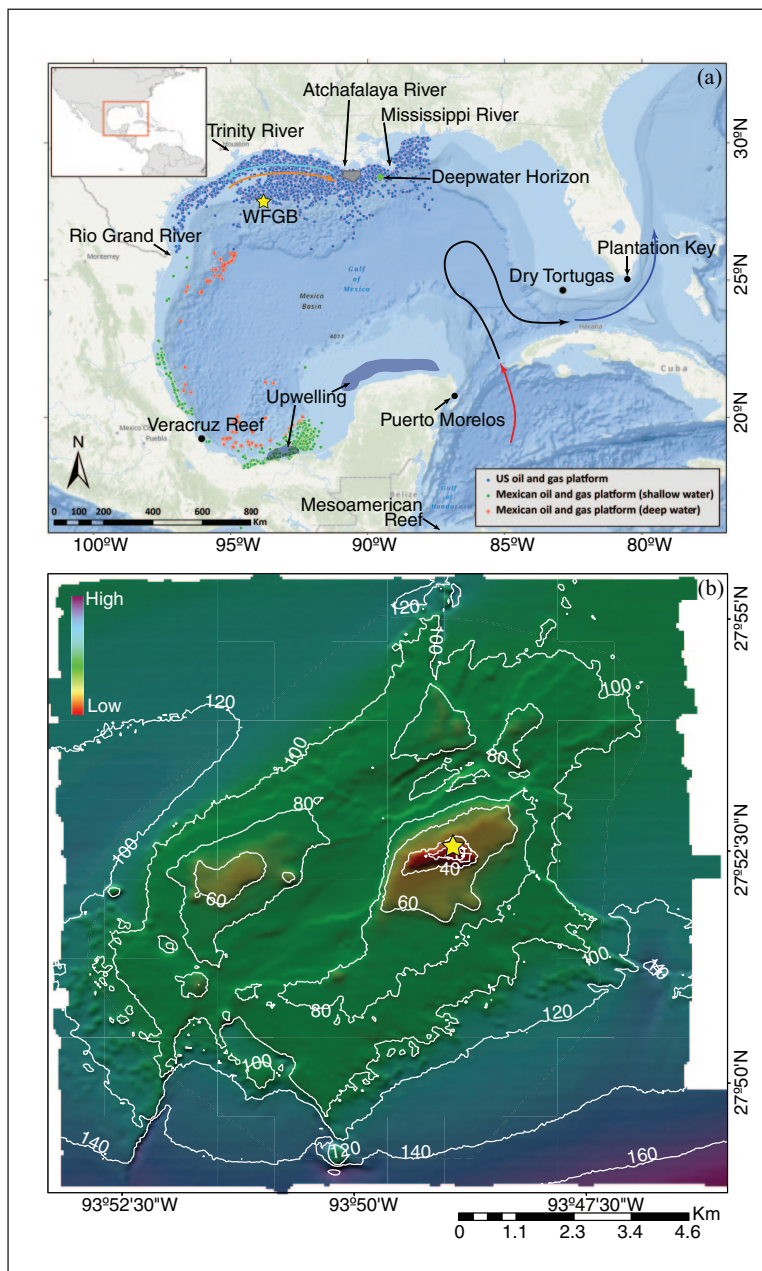
Figure 1. The location of west Flower Gaeden Bank (WFGB) (yellow ★) in the GoM of the western Atlantic Ocean: (a) bathymetry map of the GoM and its location with respect to North America (inset). Curved arrows are the approximate locations of the predominant currents, the Caribbean Current entering the GoM (red line), the Loop Current (black line) that leaves the gulf becoming the Florida Current (blue line). Seasonal northern GoM coastal currents (winter cyan arrow and summer orange arrow) transport the Mississippi and Atchafalaya Rivers' discharge along the coastline. The approximate seasonal upwelling zones are dark blue areas. Locations of the United States (US)' (www.boem.gov) and Mexico's (mapa.hidrocarburos.gob.mx) oil platforms are small circles. Locations of other relevant sites are marked (●), (b) bathymetry map of WFGB (https://pubs. usgs.gov/of/2002/0411/data.html) noting the location of the *S. siderea* colony cored for this study (yellow ★). Reproduced in color in online version.

coral reefs worldwide, due to FGB's higher latitude (~28°N), which is near the northernmost limits of coral reef-supporting conditions, and its deeper water depth (18–40 m) than most coral reefs. Fishing is restricted in the sanctuary boundaries to only conventional single hook and line gear. Divers are the typical visitors to FGBNMS and they travel there from April to July, before hurricane season peaks in August and September, and stay on live-aboard boats since the transit time is 10–12 hours. In the past 12 years (2009–2021), FGBNMS averaged about 800 divers per year, thus impacts from divers compared to other Atlantic coral reefs are minimal (personal communication Johnson 2022).

The remote location of the FGBNMS means that these coral reefs are less vulnerable than coastal coral reefs to anthropogenic pollution from the land and are less disturbed by fishing and diving; one of the requirements for the Anthropocene GSSP (Waters et al., 2023). Furthermore, this means there is no local impact or signal in the coral's skeletal geochemistry, thus corals in FGBNMS are recording environmental histories that are regional or global rather than local. The candidate site reported here is within the FGBNMS and is protected and actively managed by the National Oceanic Atmospheric Administration since 1992 with cooperation from fishermen, the oil industry, divers, and conservation groups. FGB has been studied since the 1930s with many books, papers, and annual scientific reports summarizing efforts published by FGBNMS. However, these coral reefs are not immune to anthropogenic influence. The formation of salt domes also creates space under the seabed in which oil and gas can collect. More than 9000 offshore platforms have operated in the northern GoM since 1982 (Figure 1a) and several offshore petroleum platforms have operated within 30 km of the FGB (Pulster et al., 2020), yet there have not been any documented changes in the health of the coral reef caused by oil operations (Office of National Marine Sanctuaries, 2008). Furthermore, FGBNMS was not impacted by the Deepwater Horizon oil spill in 2010, which is located ~540 km from FGBNMS (Figure 1a; Johnston et al., 2021). The FGB coral reefs exist due to the rising salt domes and the salt domes themselves are indirectly a contributing reason to the predicted demise of coral reefs due to global warming (Dee et al., 2019; Frieler et al., 2013) by providing locations for crude oil to accumulate. Paradoxically, the FGB coral reefs are perhaps the healthiest in waters of the United States (US) and the Atlantic Ocean and are poised to survive longer than other coral reefs (Lawman et al., 2022), and thus another reason why we selected WFGB as a candidate site for the Anthropocene GSSP.

Materials and methods

Geographic settings of the core site

The GoM is a semi-enclosed basin located in the western Atlantic Ocean just northwest of the Caribbean Sea surrounded by the US, Mexico, and Cuba (Figure 1a). The gulf has an area of over 1,500,000 km^2 where one-third of that area is a broad gently sloping continental shelf with a water depth of less than 200 m and also contains "salt domes" rising toward the ocean surface. Some of these submerged salt domes reach water shallow enough to have coral reefs form in the last 12,000 years after the Last Glacial Maximum when global sea level rose from the lowstand (Slowey et al., 2008).

Waters in the GoM are a mixture of riverine waters with warm and saltier waters from the Caribbean Sea, which is a mixture of North and South Atlantic waters (Wilson and Johns, 1997), brought into the gulf by the Loop Current through the Yucatan Channel and exiting through the Straits of Florida to ultimately form the Gulf Stream (Figure 1a; Alvera-Azcárate et al., 2009). The northern extent of the Loop Current varies seasonally and sheds eddies that migrate and persist for many weeks (Alvera-Azcárate et al., 2009; Sturges and Evans, 1983). The surface water temperature in the northern gulf can reach 31°C in the summer and cools to 18°C in winter.

The primary freshwater source to the GoM is the Mississippi River, which accounts for 64% of the total freshwater discharge into the GoM (Darnell and Defenbaugh, 2015) and other notable rivers near FGBNMS are the Atchafalaya, Trinity, and Rio Grande (Figure 1a). Mississippi River discharge into the northern GoM contains immense amounts of nutrients that increase primary production in the ocean surface waters and lead to eutrophication that forms one of the largest hypoxic zones in the world along the Louisiana coast (Rabalais et al., 2002). This river water moves westward along the coast by seasonally varying cross-shelf currents (Zavala-Hidalgo et al., 2014).

Field collection of core, sampling, and core imagery

A team of divers from FGBNMS, Florida Keys National Marine Sanctuary, US Geological Survey, and Texas A&M University collected coral cores from WFGB in May 2005 under permit FGBNMS-2005-002. They used an underwater hydraulic drill system with a 4-inch (101.6 mm) diameter diamond-tipped drill bit to vertically drill down from the top center of the coral colony. A 1.74 m-long cylindrical core (05WFGB3) was collected in five sections from a large boulder-shaped *S. siderea* coral colony (27.8762°N, 93.8147°W) at a water depth of 21.3 m. The coral colony is still on the reef and could be cored again with the proper permits and in cooperation with FGBNMS. The core 05WFGB3 is on loan from the FGBNMS and will ultimately be returned to them. Details on cutting the core, X-ray imaging, and preparations for extracting samples are detailed in the Supplemental Material.

Coral X-radiographs and scans were used to determine annual extension (one component of coral growth) per year, locate sampling paths, and assign years. A year was assigned to each density band couplet (light and dark) starting from the core top and counting down to the bottom of the core. The ruler tool in Adobe Photoshop was used to measure the distance from the top of successive high-density dark bands (~January) and distances were recorded in the measurement log. Three paths were measured for each slab and the results for each year were averaged together. The precision of this method is limited by the resolution of the X-radiographs, clarity of the density bands in the X-radiographs, and user experience; therefore, the precision for extension measurements was estimated by the standard error of the mean ($> \pm 0.174$ mm, 1σ).

Two sampling resolutions were used for geochemical analyses, annual for radiogenic isotopes, $\delta^{15}N$, and Hg, which require more mass, and monthly for trace elemental ratios and stable isotope ratios (Table 1). Annual coral samples were removed from coral slabs (slabs C and D) using X-radiographs to aid in cutting for each year starting in winter (assuming January) to the next year. For monthly samples, an micromill system was used to extract monthly samples (0.4 mm increment sample^{-1}) from the coral slab surface (DeLong et al., 2011; Weerabaddana et al., 2021), see Supplemental Material. Divots (1.5 mm deep) were made at every 12th sample, which are visible in the coral scans and X-radiographs, as markers to assist in assigning time to the coral geochemistry.

Chronological controls

Chronologies for corals were determined by counting annual density band couplets from the top of the core when collected live and the collection date is known (May 2005 for core 05WFGB3) down core for each density band couplet. Two coral samples were dated with high precision ^{230}Th dating ($< \pm 1$ year for corals < 100 years old) (Shen et al., 2003, 2008) (Supplemental Figure 5). U-Th isotopic analysis was conducted in the High-Precision Mass Spectrometry and Environmental Change Laboratory at National Taiwan University with a Thermo Electron Neptune multi-collector inductively coupled plasma mass spectrometer (Cheng et al., 2013; Shen et al., 2012).

Table 1. Sample details for geochemical analysis.

Analysis type	Mass (mg)	Resolution	Interval[a]	Slab[b]	Date uncertainty[c]
Radiocarbon (^{14}C)[a]	160–480	Annual	1929–2005	C	±0.1–0.2 year
Radiogenic isotopes[a] ^{137}Cs, ^{210}Pb, ^{241}Am, $^{239\text{-}240}$Pu	520–980	Annual	1929–2005	C	±0.1–0.2 year
SCP's	570–1460	Annual	1929–2005	C	±0.1–0.2 year
Pollution metal (Hg)[a]	~500	Annual	1929–2005	C	±0.1–0.2 year
Coral skeletal-δ^{15}N[d]	8	Annual	1929–2005	D	±0.1–0.2 year
δ^{18}O, δ^{13}C	0.04–0.08	Monthly	1933–2005	A	±1–2 months
		2/year	1932–1755	A	±1–2 months
Trace elements					
Sr/Ca, Mg/Ca, Ba/Ca	0.063–0.210	Monthly	1755–2005	A	±1–2 months
Li/Ca, Li/Mg, U/Ca	0.063–0.210	Monthly	1981–2005	A	±1–2 months

[a]All years were not analyzed.
[b]See Supplemental Figure 1 for core cutting and slabbing plan.
[c]Estimated sample date uncertainty. Years were cut from the coral for ~January to December.
[d]Annual samples were cut consecutively for δ^{15}N.

Time assignment for monthly data was performed with the ~monthly coral Sr/Ca using Analyseries software (Paillard et al., 1996) and then applied to the other geochemical series. Monthly Sr/Ca were aligned to a monthly sea surface temperature (SST) time series (ERSSTv3b for the 2° grid box centered on WFGB, 28°N, 94°W) (Smith et al., 2008) back to 1870 CE and then using a time series of repeating monthly SST climatology for the older coral sections. Coral Sr/Ca maxima were assigned to the coldest month each year and coral Sr/Ca minima to the warmest month each year. *S. siderea* can grow faster in summer when compared with winter; therefore, time assignment using only two tie-points per year may be biased toward the summer; therefore, mid-spring and mid-autumn tie points were used (DeLong et al., 2016). After time assignment, each time series was linearly interpolated to even monthly time intervals. The X-radiograph chronology was verified by matching the coral Sr/Ca annual cycles using the divots in the coral scans and X-radiographs.

Anthropocene proxies

Methods for radiogenic and stable isotopes and trace elements listed in Table 1 appear in Supplemental Material.

Numerical analysis

Means are reported with ±1 standard deviation. Correlation analysis is Pearson correlation using degrees of freedom. Significance of linear trends was assessed with the Mann-Kendall test (Greene et al., 2019). Change points (ischange.m in MATLAB) were detected for changes in linear slope, and/or means for a specified number of changes (Killick et al., 2012). Statistical tests assume a 5% significance level.

Results

Chronology

The entire core 05WFGB3 spans 1755–2005 CE as determined by counting annual density bands in the X-radiographs and annual cycles in monthly coral Sr/Ca and verified with two ^{230}Th dates

(Supplemental Figure 5, Supplemental Table 2). There is no evidence of diagenesis in this coral core and we find no evidence of post-depositional alteration in the X-radiographs (Supplemental Figures 2–5). The core section containing 1932–2005 (05WFGB3-1), which is the interval of interest for the GSSP markers, is continuous and has no breaks except for ones that occurred in the laboratory for which there are no missing time (Supplemental Figures 2–5). The coral X-radiographs for the three slabs have clear annual density bands that correlate among the slabs and the years are easily marked. The monthly coral Sr/Ca and δ¹⁸O variations co-vary with temperature records for FGB (see section Sr/Ca, Li/Ca, Li/Mg, and U/Ca; and Weerabaddana et al., 2021) further supporting the accurate-to-the-year chronology assignment (1932–2005 CE) for core section 05WFGB3-1. Further coral chronology results for the remainder of the core (1755–1931 CE) before the proposed Anthropocene base are located in Supplemental Material.

Calculation of growth rates

Measurements of the X-radiographs for each year resulted in an overall average annual linear extension of 5.99 ($\pm$0.61, 1σ) mm for 1928–2004 CE, the interval for Anthropocene markers in this report (Figure 2). The maximum is 7.81 mm (1934) and the minimum is 3.58 mm (1932), the year of the break between core sections, which contributed to this low extension year. There is a significant decreasing trend (0.0092 mm year^{-1}) in coral annual extension during this interval resulting in a decrease in coral growth of 0.70 mm in 76 years. The minimum annual linear extension is greater than the threshold for growth-related effects for this species ($<$1.7 mm) for coral geochemical proxies (DeLong et al., 2016; Kuffner et al., 2017); therefore, there is no concern with growth-related effects for this coral's geochemistry.

Coral colonies do not grow at a constant rate but vary year-to-year and within the colony (Figure 2, Supplemental Figure 6) because the coral colony is dome-shaped and the coral grows vertically and horizontally at different rates. Boulder-shaped massive corals have internal centimeter-scale growth structures that can vary within the colony; however, *S. siderea* has relatively simple internal structures compared to other Atlantic massive coral species and thus has more internally reproducible geochemical records that result in robust geochemical time series (DeLong et al., 2011, 2016). Coral annual density couplets visible in X-radiographs provide highly accurate chronologies with continuous deposition of the coral skeleton with rare occurrences of missing and false years as are found in tree-ring chronologies (Black et al., 2019; DeLong et al., 2013).

Radioisotopes (and guidance for other proxies)

Radiocarbon – Core 05WFGB3 exhibits low (−50‰) Δ¹⁴C from 1920 to 1957 CE followed by an increase observed after 1957 (depth from core top to January 1957 = 284.1 mm) with the largest year-to-year increase occurring from 1961 to 1962 and increasing to a maximum in 1970 CE (depth = 207.2 mm) (Figure 2, Table 2, Supplemental Figure 7). For change point analysis (Killick et al., 2012), we tested 1 to 4 change points and found consistent results. We found this analysis is sensitive to the direction of the time series and results vary by 1 year; we used the earliest year for the proposed Anthropocene marker. The coral Δ¹⁴C represents the transfer of the atmospheric Δ¹⁴C signal to the surface ocean (i.e. the actual bomb peak observed in the atmosphere after 1954 in the northern hemisphere and 1955 in the southern hemisphere).

We compared core 05WFGB3 ¹⁴C results to two *Orbicella faveolata* coral records (Wagner, 2011), one in the WFGB close to the coral where the core 05WFGB3 was extracted from and the other from Santiaguillo Reef offshore from Veracruz, Mexico in the southern GoM, both sampled with annual resolution (Figures 1a and 3). The Veracruz coral Δ¹⁴C closely tracks the WFGB coral
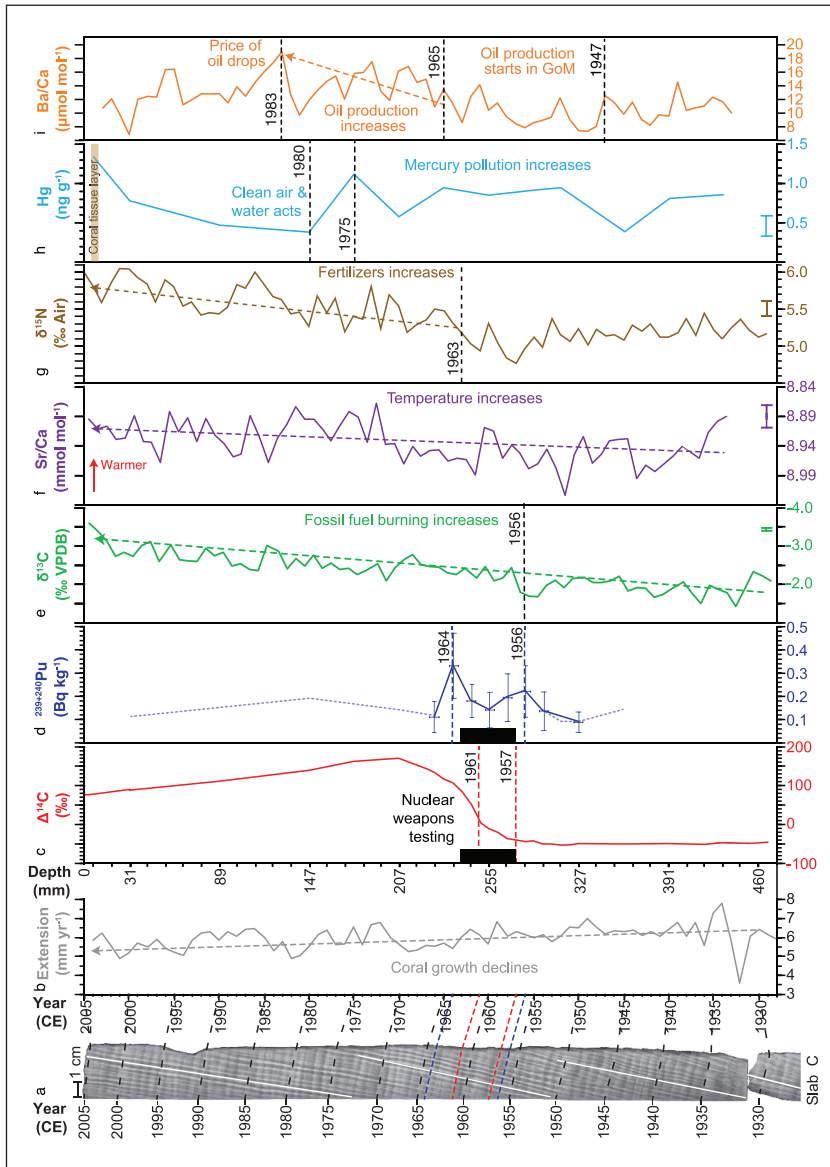
Figure 2. Composite of annually-resolved proxies from core 05WFGB3: (a) X-radiograph of slab C with examples of counting path (white lines) and every 5 years noted (labels on ~January) connected to (b) years in the coral annual extension (black dashed lines). Years for the proposed base of the Anthropocene markers are noted as red dashed lines in (a and c) and secondary marker with blue dashed lines in (a and d) with blue dotted line is limit of detection values (sample activity is less than this value) rather than actual measured activity. (b) Annual extension was determined from coral growth direction noted as white lines in (a). Depth from core top for (c–i) is aligned with extension (b) and years (a) with depth noted for January of each year or the base of the annual sample for the annually-sampled proxies (c, d, g, and h) and the annual average from monthly samples (e, f, and i). Black boxes span 1957–1963, the period of extensive atmospheric thermonuclear weapons testing (c and d). Linear trends (dashed lines with arrowheads) are significant (1%). Error bars represent analytical precision (1σ) and if not plotted analytical precision is smaller than the line weight. Dating uncertainties for each proxy are given in Table 1. Reproduced in color in online version.

Table 2. Radiocarbon measurements for core 05WFGB3 carbonate analysis.

Sample[a] depth (mm)	Sample code[b]	ETH-	^{14}C age (BP)[c]	±1σ	$F^{14}C$[d]	±1σ	$δ^{13}C$[e] (‰ VPDB)	±1σ	C (mg)
0.0–3.4	05WFG-3 Year: 2005	ETH-117559	−643	21	1.083	0.0029	−3.4	1.0	0.96
3.4–9.4	05WFG-3 Year: 2004	ETH-117560	−654	22	1.085	0.0029	−2.4	1.0	0.95
26.1–31.2	05WFG-3 Year: 2000	ETH-117561	−745	22	1.097	0.0030	1.2	1.0	0.56
26.1–31.2	05WFG-3 Year: 2000	ETH-117561	−732	22	1.095	0.0030	−3.2	1.0	0.95
82.7–88.5	05WFG-3 Year: 1990	ETH-117562	−889	21	1.117	0.0030	−4.8	1.0	0.86
141.0–146.6	05WFG-3 Year: 1980	ETH-117563	−1079	21	1.144	0.0030	−4.1	1.0	0.96
170.9–177.4	05WFG-3 Year: 1975	ETH-117564	−1235	21	1.166	0.0031	−3.7	1.0	0.96
202.2–207.2	05WFG-3 Year: 1970	ETH-117565	−1283	21	1.173	0.0031	−2.9	1.0	0.95
217.8–223.7	05WFG-3 Year: 1967	ETH-117566	−1096	22	1.146	0.0031	−2.8	1.0	0.95
223.7–229.1	05WFG-3 Year: 1966	ETH-117567	−1033	21	1.137	0.0030	−4.1	1.0	0.96
229.1–234.9	05WFG-3 Year: 1965	ETH-117568	−905	22	1.119	0.0030	−3.4	1.0	0.96
234.9–240.0	05WFG-3 Year: 1964	ETH-117569	−832	22	1.109	0.0030	−2.3	1.0	0.96
240.0–245.9	05WFG-3 Year: 1963	ETH-117570	−661	22	1.086	0.0029	−2.1	1.0	0.95
245.9–252.6	05WFG-3 Year: 1962	ETH-117571	−416	22	1.053	0.0027	−2.1	1.0	0.96
252.6–259.1	05WFG-3 Year: 1961	ETH-117572	−39	22	1.005	0.0027	−2.4	1.0	0.96
259.1–254.7	05WFG-3 Year: 1960	ETH-117573	72	22	0.991	0.0027	−2.7	1.0	0.96
264.7–271.7	05WFG-3 Year: 1959	ETH-117574	152	22	0.981	0.0027	−2.2	1.0	0.96
271.7–277.9	05WFG-3 Year: 1958	ETH-117575	282	22	0.965	0.0026	−3.2	1.0	0.90
277.9–284.1	05WFG-3 Year: 1957	ETH-117576	319	22	0.961	0.0026	−2.5	1.0	0.92
284.1–290.3	05WFG-3 Year: 1956	ETH-117577	352	22	0.957	0.0026	−2.9	1.0	0.95
290.3–296.6	05WFG-3 Year: 1955	ETH-117578	349	22	0.958	0.0026	−2.2	1.0	0.96
269.6–302.0	05WFG-3 Year: 1954	ETH-117579	414	22	0.950	0.0026	−3.0	1.0	0.95
302.0–307.7	05WFG-3 Year: 1953	ETH-117580	411	22	0.950	0.0025	−3.9	1.0	0.95
307.7–313.8	05WFG-3 Year: 1952	ETH-117581	440	22	0.947	0.0026	−2.1	1.0	0.95
313.8–320.3	05WFG-3 Year: 1951	ETH-117582	432	22	0.948	0.0026	−1.9	1.0	0.95
320.3–326.9	05WFG-3 Year: 1950	ETH-117583	401	22	0.951	0.0026	−2.1	1.0	0.96
353.9–360.4	05WFG-3 Year: 1945	ETH-117584	419	22	0.949	0.0026	−1.5	1.0	0.95
384.6–391.1	05WFG-3 Year: 1940	ETH-117585	411	22	0.950	0.0026	−2.1	1.0	0.96
410.8–416.0	05WFG-3 Year: 1936	ETH-117586	438	22	0.947	0.0026	−1.9	1.0	0.95
416.0–423.4	05WFG-3 Year: 1935	ETH-117587	418	22	0.949	0.0026	−2.3	1.0	0.95
423.4–431.1	05WFG-3 Year: 1934	ETH-117588	400	22	0.951	0.0026	−2.6	1.0	0.95
447.0–453.7	05WFG-3 Year: 1930 (1931)	ETH-117589	405	22	0.951	0.0026	−2.1	1.0	0.95
453.7–460.0	05WFG-3 Year: 1929 (1930)	ETH-117590	402	22	0.951	0.0026	−2.3	1.0	0.96
460.0–465.7	05WFG-3 Year: 1928 (1929)	ETH-117591	389	22	0.953	0.0026	−0.8	1.0	0.96

[a]Depth range for each ^{14}C annual sample starting from top of coral core (05WFGB3 Slab C) measured on X-radiographs.

[b]Years in parentheses are the actual years determined by counting coral Sr/Ca cycles, annual density bands and ^{230}Th dating. The dates were adjusted between core section 3-1 and 3-2 after samples for radiocarbon were cut. Years were cut from the coral for ~January to December for each year (Table 1).

[c]BP = Before Present (before 1950 CE)

[d]$F^{14}C$ is fraction modern determined as $\exp(-^{14}C \text{ age}/8033)$ (Reimer 2004). If $F^{14}C > 1$, the sample indicates presence of bomb peak ^{14}C (post 1950 CE).

[e]$δ^{13}C$ is a value measured on graphite and might include additional fractionation.
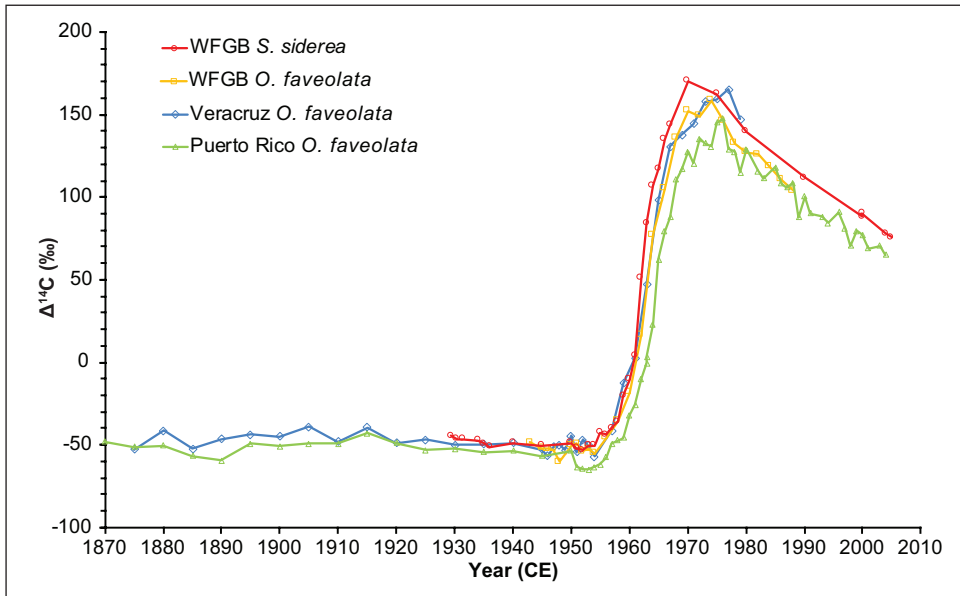
Figure 3. Coral core 05WFGB3 Δ^{14}C values compared with select corals from the tropical Atlantic Ocean (Kilbourne et al., 2007; Wagner, 2011). Coral Δ^{14}C records were not adjusted for the Suess effect. Dating and Δ^{14}C uncertainties (2‰–3‰) are about the size of the hollow circle (Table 1). Reproduced in color in online version.

Δ^{14}C of the same species. There is a 4–7 year difference in the maximum Δ^{14}C peaks between the species and the maximum Δ^{14}C values differ by 11.8‰ with *S. siderea* having higher maximum values. The rapid increases or "bomb spikes" in all three of these coral Δ^{14}C records occur in the same years within the sampling uncertainty (± 0.5 year), suggesting differences in coral species are not influencing these Δ^{14}C results.

The Δ^{14}C bomb peak in various parts of the world's oceans can have different shapes due to each part of the ocean having different patterns of mixing water. The radiocarbon bomb peak was used to untangle this information (Broecker and Peng, 1982). Surface ocean Δ^{14}C values are the result of equilibration with the atmosphere; however, upwelling, advection, and other mixing processes can influence oceanic Δ^{14}C (Mahadevan, 2001). In the northwestern GoM, weak springtime upwelling events (days–weeks) of waters as deep as 200 m can occur along the continental shelf edge, where FGB is located, when the winds reverse in the spring (Murray et al., 1998; Teague et al., 2013). However, daily reef temperature measurements in FGB (Johnston et al., 2021) do not show evidence of cold water upwelling on the reef (the coldest daily temperature was 17.6°C between 1986 and 2014). Furthermore, hermatypic (reef-building) corals generally cannot tolerate temperatures <17°C, thus regular upwelling would impact the development of a coral reef in this location if it was occurring. These short-term upwelling events should not impact coral Δ^{14}C sampled with annual resolution (i.e. each sample represents the annual average Δ^{14}C).

A comparison with an *O. faveolata* from the southern coast of Puerto Rico (Kilbourne et al., 2007) finds similar timing for the Δ^{14}C increases due to weapons testing (Figure 3). However, the WFGB Δ^{14}C record does not contain the Δ^{14}C depletion event between 1950 and 1953 seen in Puerto Rico and other Caribbean sites due to the mixing of low Δ^{14}C equatorial Atlantic surface waters in the Caribbean Sea (Kilbourne et al., 2007). This depletion event reduces the Δ^{14}C values for Puerto Rico creating a visual shift in the figure but the timing of the increase in Δ^{14}C is the

Table 3. $^{239+240}$Pu for core 05WFGB3.

Sample depth[a] (mm)	Sample year[b]	$^{239+240}$Pu (Bq kg^{-1})	$\pm$[c] $k=2$
26.1–31.2	2000	0.108	
141.0–146.6	1980	0.188	
202.2–207.2	1970	0.138	
223.7–229.1	1966	0.114	0.068
234.9–240.0	1964	0.336	0.141
245.9–252.6	1962	0.184	0.072
259.1–264.7	1960	0.145	0.077
271.7–277.9	1958	0.198	0.103
284.1–290.3	1956	0.225	0.112
296.6–302.0	1954	0.140	0.083
307.7–313.8	1952	0.088	
320.3–326.9	1950	0.092	0.044
353.9–360.4	1945	0.139	
410.8–416.0	1936	0.085	

[a]Depth range for each annual sample starting from top of coral core (05WFGB3 Slab C) measured on X-radiographs.
[b]Each sample represents one year of coral growth for ~January to December (Table 1).
[c]Data points with no error bars indicate limit of detection values (i.e. sample activity is less than this value) rather than actual measured activity.

same. The lack of this depletion event in the GoM coral Δ^{14}C records suggests that when the Caribbean waters reach the GoM this lower Δ^{14}C equatorial water has been mixed with other water and/or equilibrated with atmospheric ^{14}C sources; therefore, the GoM represents a more global signal.

Plutonium – The $^{239+240}$Pu activities show marked increases in 1956 (depth from core top to January 1956 = 290.3 mm) and 1964 (depth = 240.0 mm) that follow periods of increased atmospheric thermonuclear weapons testing in the early 1950s and 1961–1963 (Figure 2, Table 3, Supplemental Figure 8). Plutonium was not detectable in pre-1950 samples. There is a decline in $^{239+240}$Pu activities after 1964, with activities for coral samples dated to 1970, 1980, and 2000 being below detection limits. Unlike Δ^{14}C, only 14 samples from the interval 1936–2000 were analyzed for $^{239+240}$Pu, and for 1950–1966 every other year was analyzed; therefore, it is possible greater $^{239+240}$Pu peaks could have occurred in odd-numbered years that were not analyzed. This study also examined $^{239+240}$Pu yearly from 1950–1959 in coral from Haiti (10LEO1) growing at the water surface (Supplemental Table 9) that has a peak in 1956.

Plutonium fallout from weapons testing has spread worldwide, mostly in the northern hemisphere, where more testing occurred, but was also affected by test location, wind and precipitation patterns, ocean currents, and water depth (Sanchez-Cabeza et al., 2021). A scaled comparison with other coral $^{239+240}$Pu studies to highlight maximum values (Figure 4) shows the Pacific corals, especially those near the Pacific Proving Grounds testing sites (Enewetak and Bikini) have maximum $^{239+240}$Pu values occurring before the Atlantic corals. Atlantic corals tend to record maximum $^{239+240}$Pu activities in the early-mid 1960s following the 1963 global fallout maximum (Sanchez-Cabeza et al., 2021). The exception is the Haiti coral (10LEO1) that has a maximum in 1956. However, this is an artifact of the figure since we scaled by the maximum value for each core and Haiti did not have a sample measured between 1959 and 1970 and thus is missing the 1964 peak. The coral species may also play a role as the other Atlantic corals are *Orbicella* sp. and corals 05WFGB3 and 10LEO1 are *S. siderea*, both of which have higher $^{239+240}$Pu activities than the
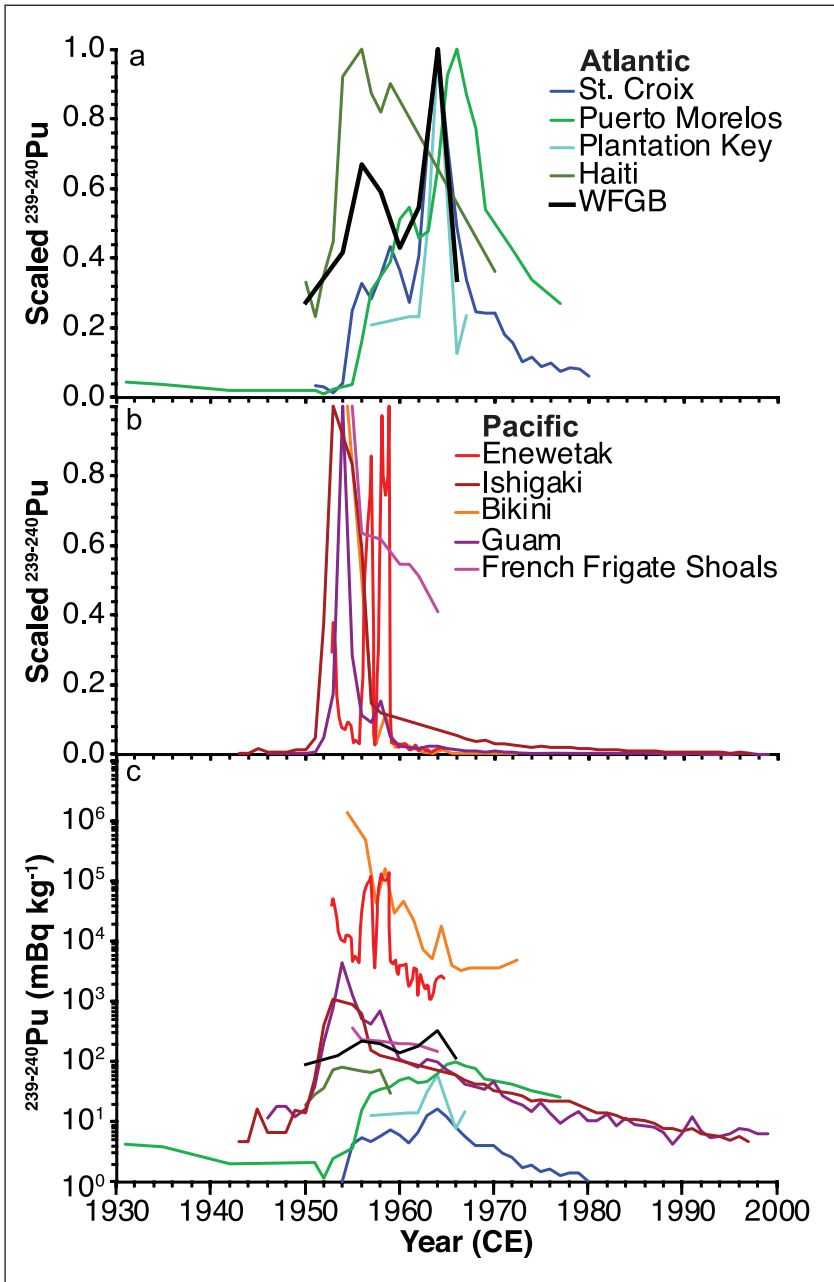
Figure 4. Summary of coral $^{239+240}$Pu studies. (a and b) Plutonium is scaled by the maximum activity of each record and is unitless; modified from Sanchez-Cabeza et al. (2021) Pacific sites (a) are warm colors and Atlantic sites (b) are cool colors. (c) Plutonium activities for each record not scaled using the same color labels as in (a) and (b). Sites are Bikini (Noshkin et al., 1975), Enewetak (Froehlich et al., 2017), Guam (Lindahl et al., 2011), Ishigaki (Lindahl et al., 2012), Hawaii (Buesseler, 1997), Croix (Benninger and Dodge, 1986), Plantation Key (Purdy et al., 1989), Morelos (Sanchez-Cabeza et al., 2021), Haiti (10LEO1; Supplemental Table 9), and WFGB (this study). Reproduced in color in online version.

Orbicella studies (Figure 4c). *S. siderea* is a coral with a dense skeleton and is relatively slow growing so it may take up and store Pu in its skeleton more readily than the less dense *Orbicella* corals.

Other artificial fallout radionuclides – No ^{137}Cs and [241]Am were detected in the core 05WFGB3 samples (Supplemental Results, Supplemental Table 4).

Novel materials

*Spheroidal carbonaceous fly-ash particles (SCPs)* – No SCPs were found in the 33 coral samples from core 05WFGB3 (Supplemental Results, Supplemental Figure 9, Supplemental Table 5).

Geochemical proxies for climate

Oxygen isotopes – The monthly-resolved coral $\delta^{18}O$ have clear seasonal cycles that significantly co-vary with temperature (Supplemental Figure 10, Supplemental Table 6) that were averaged annually (January–December) to assess trends. The annual average coral $\delta^{18}O$ record has a significant trend toward lower values for the interval from 1932 to 2005 CE indicating lower temperatures and/or saltier conditions similar to the interval from 1826 to 1890 CE (Figure 5a). Instrumental and other coral proxies reconstructions suggest the GoM is warming during the 20th century (Allard et al., 2016; DeLong et al., 2014; Flannery et al., 2017); therefore, we interpret this trend as the northern GoM is becoming saltier. Coral $\delta^{18}O$ is an important hydroclimate proxy that can provide insights into moisture flux from the ocean to the atmosphere and freshwater entering the ocean. Coral $\delta^{18}O$ by itself is not a marker for the Anthropocene but can inform us of the response of the climate system to anthropogenic forcing.

Sr/Ca, Li/Ca, Li/Mg, and U/Ca – We evaluated several coral temperature proxies from 1986 to 2005 CE and assessed the skill of the temperature reconstructions with reef temperature measurements from WFGB (Johnston et al., 2021) and OISST, a 1° gridded and interpolated data product that includes satellite-derived estimates of monthly SST for complete coverage (Reynolds et al., 2002). The monthly coral Sr/Ca, Li/Ca, Li/Mg, and U/Ca records have clear seasonal cycles that are significantly co-varying with temperature (Supplemental Figure 10, Supplemental Table 6). Coral Sr/Ca analyzed with ICP-OES has the highest correlation with reef temperature and OISST and is the best-performing coral temperature proxy (error of reconstruction = 1.27°C). Coral Sr/Ca analyzed with ICP-OES has a better analytical precision than ICP-MS (Supplemental Table 1) likely due to isotopic interferences in the plasma. For the rest of the core 05WFGB3, we analyzed monthly Sr/Ca using ICP-OES and then determined annual averages (January–December) to assess long-term trends.

The annually-resolved coral Sr/Ca record has a significant linear decrease of 0.048 mmol mol^{-1}, equivalent to an increasing trend of 1.1°C, for the interval from 1932 to 2005 CE, similar to the global warming trend (Figures 2 and 5c), using the coral Sr/Ca-SST calibration equation determined for this coral (Weerabaddana et al., 2021). The interval from 1940 to 1970 CE has cooler SST with warmer SST after 1970. The interval from 1755 to 1880 CE, part of the Little Ice Age, is cooler than 1880–2005 CE with the coldest decades occurring between 1810 and 1880 CE when explosive volcanic eruptions cool global temperatures. Like coral $\delta^{18}O$, coral Sr/Ca is an important climate proxy that provides insights into past temperature variability. It is not an Anthropocene marker in itself but indicates the climate response to anthropogenic forcing. Additionally, coral Sr/Ca is useful for confirming the annual density band chronology by determining if a year is present when a band is not clear in the X-radiograph and for assessing temporal overlaps in core breaks.
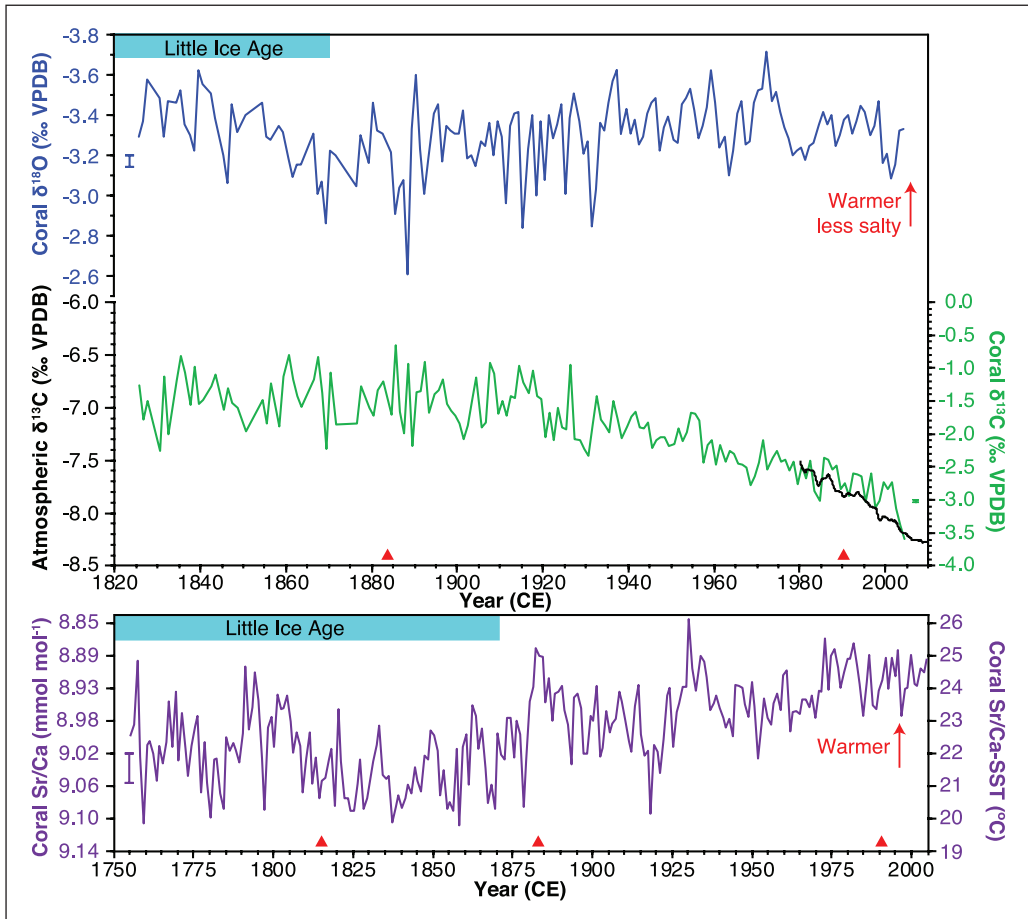
Figure 5. Annual average coral environmental markers from core 05WFGB3 for coral (a) $\delta^{18}O$, (b) $\delta^{13}C$, and (c) Sr/Ca. Monthly coral $\delta^{18}O$ and $\delta^{13}C$ values were averaged in the interval from 1932–2005 and annual maximum and minimum $\delta^{18}O$ and $\delta^{13}C$ values were averaged in the interval from 1826–1932. Monthly coral Sr/Ca variations were annually-averaged in the interval from 1755–2005. (b) Atmospheric $\delta^{13}C$ is from Mauna Loa, Hawaii is shown with the quasi-regular seasonal cycle removed (Keeling et al., 2001). (c) Coral Sr/Ca was converted to SST using the coral Sr/Ca-SST equation for this coral (Weerabaddana et al., 2021). Coral $\delta^{18}O$ and Sr/Ca are scaled to the same temperature range and plotted so that warmer values are up. Error bars (1σ) are analytical precision determined for monthly samples. For Sr/Ca precision, PL precision is plotted (Supplemental Table 1). Reproduced in color in online version.

Organic matter proxies

Carbon isotopes – The annually-resolved coral $\delta^{13}C$ averages −1.43‰ in the 1800s with a significant decreasing trend starting in the interval between 1906 and 1913 CE (results of change point analysis varies based on the number of change points) that accelerates from 2000 to 2005 CE to an average value of −3.14‰ (Figures 2 and 5b). This trend is called the "Suess effect" (Keeling, 1979) to describe the addition of CO_2 to the atmosphere from burning fossil fuels with lower $\delta^{13}C$ values compared to preindustrial levels. A comparison with atmospheric $\delta^{13}C$ measurements in Hawaii (1980–2005) (Keeling et al., 2001) finds a decrease of 0.67‰ while coral $\delta^{13}C$ declines by 1.12‰ for the same time interval, thus the coral 05WFGB3 is capturing global trends in $\delta^{13}C$ and

Table 4. Nitrogen isotope ratios for core 05WFGB3.

Sample	Sample depth (mm)[a]	Year[b]	N content (nmol mg^{-1})	δ^{15}N (‰ Air)
GB05	0.0–3.6	2005	1.31	6.01
GB04	3.6–9.7	2004	1.38	5.81
GB03	9.7–16.1	2003	1.56	5.59
GB02	16.1–21.5	2002	1.50	5.85
GB01	21.5–26.8	2001	1.37	6.04
GB00	26.8–32.3	2000	1.49	6.04
GB99	32.3–38.0	1999	1.46	5.92
GB98	38.0–43.1	1998	1.43	5.84
GB97	43.1–49.2	1997	1.66	5.60
GB96	49.2–54.5	1996	1.69	5.90
GB95	54.5–59.9	1995	1.42	5.81
GB94	59.9–64.9	1994	1.60	5.54
GB93	64.9–70.9	1993	1.47	5.59
GB92	70.9–76.7	1992	1.43	5.42
GB91	76.7–83.4	1991	1.59	5.45
GB90	83.4–88.9	1990	1.44	5.43
GB89	88.9–95.6	1989	1.50	5.52
GB88	95.6–102.0	1988	1.65	5.83
GB87	102.0–108.4	1987	1.65	5.78
GB86	108.4–114.7	1986	1.47	6.00
GB85	114.7–120.5	1985	1.61	5.84
GB84	120.5–125.9	1984	1.72	5.67
GB83	125.9–131.7	1983	1.56	5.63
GB82	131.7–136.8	1982	1.39	5.44
GB81	136.8–142.2	1981	1.60	5.46
GB80	142.2–147.8	1980	1.82	5.26
GB79	147.8–153.7	1979	1.62	5.68
GB78	153.7–160.0	1978	1.51	5.46
GB77	160.0–165.3	1977	1.25	5.65
GB76	165.3–170.9	1976	1.51	5.20
GB75	170.9–177.7	1975	1.64	5.40
GB74	177.7–183.7	1974	1.79	5.36
GB73	183.7–190.5	1973	1.27	5.81
GB72	190.5–197.4	1972	1.43	5.23
GB71	197.4–203.4	1971	1.49	5.69
GB70	203.4–208.8	1970	1.45	5.54
GB69	208.8–214.2	1969	1.35	5.19
GB68	214.2–219.3	1968	1.52	5.29
GB67	219.3–224.4	1967	1.25	5.36
GB66	224.4–230.2	1966	1.38	5.50
GB65	230.2–236.2	1965	1.53	5.47
GB64	236.2–242.0	1964	1.44	5.32
GB63	242.0–248.0	1963	1.46	5.17
GB62	248.0–254.1	1962	1.34	5.04
GB61	254.1–260.0	1961	1.63	4.94
GB60	260.0–266.2	1960	1.90	5.31

(Continued)

Table 4. (Continued)

| Sample	Sample depth (mm)[a]	Year[b]	N content (nmol mg^{-1})	δ^{15}N (‰ Air)
GB59	266.2–272.4	1959	1.49	5.04
GB58	272.4–278.4	1958	1.27	4.84
GB57	278.4–284.7	1957	1.53	4.77
GB56	284.7–291.3	1956	1.59	4.96
GB55	291.3–297.2	1955	1.59	5.12
GB54	297.2–303.6	1954	1.47	4.98
GB53	303.6–309.3	1953	1.42	5.37
GB52	309.3–315.2	1952	1.26	5.15
GB51	315.2–321.2	1951	1.24	5.06
GB50	321.2–327.8	1950	1.33	5.24
GB49	327.8–334.7	1949	1.60	5.02
GB48	334.7–341.4	1948	1.62	5.23
GB47	341.4–347.8	1947	1.55	5.14
GB46	347.8–354.1	1946	1.41	5.15
GB45	354.1–360.3	1945	1.70	5.08
GB44	360.3–367.0	1944	1.53	5.29
GB43	367.0–373.2	1943	1.68	5.21
GB42	373.2–379.2	1942	1.83	5.30
GB41	379.2–385.4	1941	1.68	5.13
GB40	385.4–391.9	1940	1.81	5.12
GB39	391.9–398.6	1939	1.62	5.18
GB38	398.6–404.6	1938	1.48	5.37
GB37	404.6–411.1	1937	1.51	5.15
GB36	411.1–417.1	1936	1.35	5.45
GB35	417.1–423.9	1935	1.59	5.22
GB34	423.9–431.4	1934	1.65	5.10
GB33	431.4–434.4	1933	1.56	4.88
GB32	434.4–437.5	1932.5	1.37	5.25
GB31	437.5–441.0	1932	1.61	5.36
GB30	441.0–447.3	1931	1.85	5.22
GB29	447.3–453.7	1930	1.76	5.12
GB28	453.7–459.9	1929	1.80	5.17

[a]Depth range for each annual sample starting from top of coral core (05WFGB3 Slab D) measured on X-radiographs.
[b]Each sample represents one year of coral growth for ~January to December (Table 1). The dates for samples GB32 to GB28 were adjusted between core sections 3-1 and 3-2 after samples were cut for analysis.

CO_2 but with a higher rate of decline. A comparison with Atlantic coral and sclerosponge δ^{13}C records (1800–2000 CE) finds similar trends with more rapid decreases in the oceans due to a greater amount of CO_2 in the surface oceans and that the rate of decline is accelerating at the end of the 20th century (Swart et al., 2010). This new coral δ^{13}C record extended to 2005 confirms further acceleration. There are slightly different δ^{13}C timings in trends for South Pacific coral δ^{13}C records, but the overall trends are similar (Dassié et al., 2013).

Coral skeleton nitrogen isotopes (CS-δ^{15}N) – The annually-resolved CS-δ^{15}N record for core 05WFGB3 contains stable values from 1928 to 1962 CE centered at 5.1‰ ± 0.15‰ followed by a significant increasing trend starting in 1963 (0.13‰ decade^{-1} for 1963–2005) (Figure 2, Table 4,
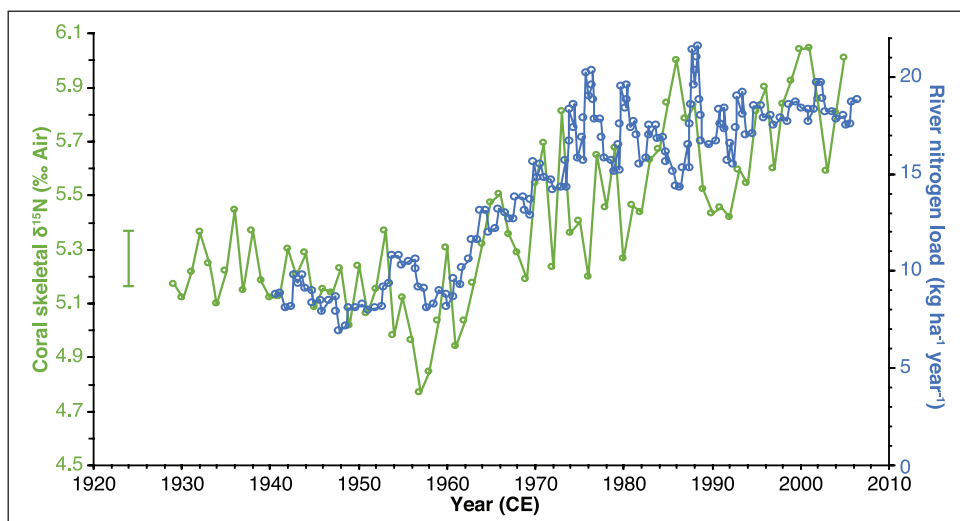
Figure 6. Comparison of CS-δ^{15}N and Mississippi River Basin nitrogen load (David et al., 2010). Error bar is analytical precision (1σ) and years are assessed to be accurate. Reproduced in color in online version.

Supplemental Figure 11). The CS-δ^{15}N is a robust indicator of the sources of nitrogen present in the surrounding environment (Duprey et al., 2017, 2020; Erler et al., 2015; Wang et al., 2016, 2018).

With values ranging from 4.8‰ to 6.0‰, the 05WFGB3 CS-δ^{15}N record is well-constrained by two end-members: the SubTropical Underwater (STUW) and the Mississippi and Atchafalaya River System (MARS) (see Supplemental Results for the definitions of the end-members). Changes in the CS-δ^{15}N can be interpreted as a change in the respective contribution of the STUW and the MARS to the GoM. The increase in CS-δ^{15}N values observed from the 1960s onward points toward a greater contribution of MARS-derived nitrogen to WFGB. Indeed, the coral record tracks remarkably the nitrogen load within the Mississippi River Basin (Figure 6) that almost doubles from the pre-1960s to 2000s with a ~0.7‰ increase during the same period. This interpretation is consistent with the increase in bulk δ^{15}N observed in the GoM for the 20th century in sediment cores (Rosenbauer et al., 2009) and deep-sea coral records (Prouty et al., 2014) that is attributed to increased nutrient loading from the MARS. See additional CS-δ^{15}N results in the Supplemental Materials.

Inorganic geochemical signals

Lead-210 activity – The low total ^{210}Pb activities from the core 05WFGB3 and the disequilibrium give ^{210}Pb high uncertainties (Supplemental Table 7) and are not deemed an Anthropocene marker for this coral, see Supplemental Results.

Mercury – Mercury concentrations in the samples from the core 05WFGB3 are low and vary from 0.38 to 1.34 ng g^{-1} with a lower value in 1945 at the end of World War II that increases until 1980 when the lowest Hg value occurs (Figure 2, Supplemental Figure 12, Supplemental Table 8). The topmost sample (2005 CE) includes residues from the coral tissue layer and thus this higher value represents the uptake of Hg by the living coral that is not incorporated into the coral skeleton. A study of *Porites astreoides* found that 96% of Hg is taken up by living tissue and only 4% was found in the coral skeleton (Bastidas and García, 2004).
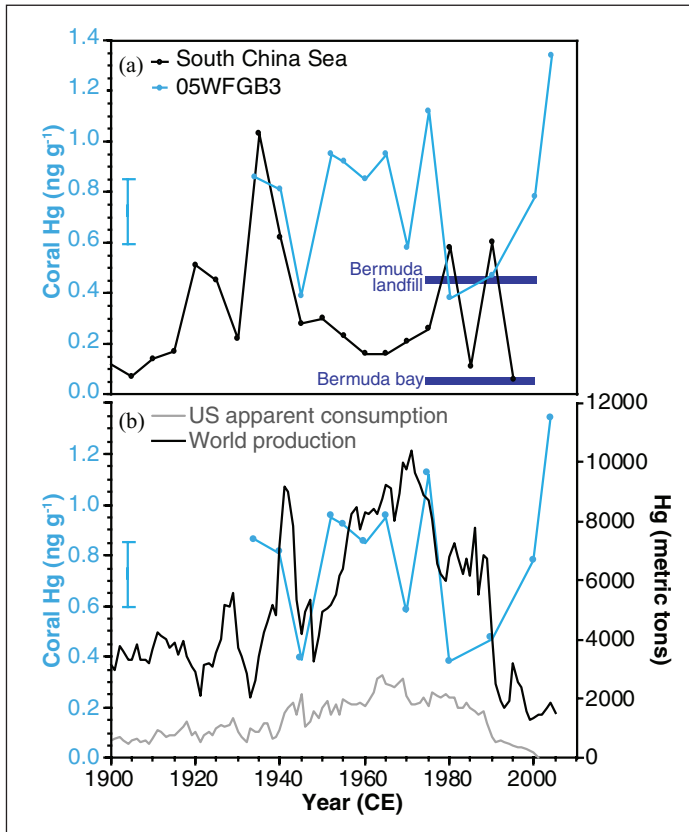
Figure 7. (a) Comparison of coral Hg skeletal concentrations with core 05WFGB3. Two coral Hg averages (1974–1994; dark blue squares) from Bermuda show differences between a relatively open ocean location and a coral growing near a landfill (Prouty et al., 2013). The South China Sea record has samples spanning 5-years and is plotted in the center of each 5-year interval (Sun et al., 2016). (b) US apparent consumption and world production of Hg (Kelly and Matos, 2014) compared with coral 05WFGB3 Hg concentration. WFGB samples are from 1 year but analyzed ~5-year intervals (Supplemental Table 8). Error bar is analytical precision (1σ) and years are assessed to be accurate. Reproduced in color in online version.

The Hg concentration in core 05WFGB3 is lower by an order of magnitude than that found in *S. siderea* corals near industrial sites in Central America (Guzmán and García, 2002) suggesting locations near pollution sources increase coral skeletal Hg concentration. Similar results were found in Bermuda for *Diploria labyrinthiformis* corals sampled near a landfill versus a nearby open bay (Prouty et al., 2013) with the WFGB coral having similar Hg concentrations as the corals near that landfill (Figure 7). A 200-year-long record of coral Hg from the South China Sea (Sun et al., 2016) has a lower baseline Hg concentration than core 05WFGB3 with a similar maximum Hg concentration; however, these two records are not co-varying. That study found increases in coral Hg are associated with Chinese wars. Core 05WFGB3 shows some co-variance with US apparent consumption and global production of Hg (Kelly and Matos, 2014) (Figure 7b). The US and other countries enacted pollution regulations in the 1960s and 1970s thus contributing to the reduction in Hg production and consumption and possibly the reduced Hg levels seen in the coral samples for 1980, 1990, and 2000 CE. The results suggest core 05WFGB3 may be recording the

US and global Hg fluctuations within the resolution of these records yet further analysis, preferably annually, would help further resolve the coral Hg signal.

Barium – The monthly-resolved coral Ba/Ca record has clear seasonal cycles that do not significantly co-vary with temperature (Supplemental Figure 10). The coral Ba/Ca results presented here build upon the study of Weerabaddana et al. (2021) that revealed the seasonal cycle in monthly coral Ba/Ca is mostly driven by surface ocean productivity. Furthermore, that study found the GoM has some of the highest coral Ba/Ca values globally. The annually-averaged coral Ba/Ca contains a significant difference in mean coral Ba/Ca of 1.57 μmol mol^{-1} between 1933–1947 and 1948–2004, pre- and post-oil extraction operations in the GoM, respectively. There is a significant increasing trend from 1965 to 1983 (these years are change points along with 1947; Figure 2). Generally, coral Ba/Ca records upwelling or riverine sedimentation in the coastal environment (Alibert et al., 2003; Lea et al., 1989); however, WFGB is not close enough to a river source or upwelling that would influence coral Ba/Ca. However, the GoM is home to extensive ocean drilling operations that use barite (BaSO$_4$) as drilling muds and has many offshore oil platforms (Figure 1a) that discharge production waters that contain barite into the gulf (Bleiwas and Miller, 2015). The US barite production and consumption can be used as a proxy for barite input to the oceans (Kelly and Matos, 2014) since >90% of barite produced in the US are used for offshore oil drilling (Bleiwas and Miller, 2015) and the GoM is the primary oil field for the US. Barite production and consumption peaks in 1981 with a sharp decline afterward with falling oil prices and coral Ba/Ca captures this peak in 1983 with a three-year delay due to barite production stockpiles taking time to be shipped to the offshore drilling platforms before being used as drilling mud (Weerabaddana et al., 2021).

Discussion

We propose the coral core 05WFGB3 as the Anthropocene GSSP and this discussion will address the requirements for a GSSP that applies to the Anthropocene (Head and Gibbard, 2015; Waters et al., 2023). The core 05WFGB3 provides a record of a primary Anthropocene marker, the Δ^{14}C bomb spike starting in 1957 CE, and secondary markers in the 20th century, the $^{239+240}$Pu bomb spikes in 1956 and 1964, that can be accurately dated to the year and correlated with global anthropogenic signals (Figure 2). The core 05WFGB3 is 1.74 m long and is comprised of primary aragonite with no signs of diagenesis, bioerosion, or disturbances in the core except for breaks that occur during coring or during cutting the core into slabs for X-radiographs and geochemical sampling (Supplemental Figures 1–5). The regular monthly coral Sr/Ca and Mg/Ca signals also support the pristine nature of this core since anomalies in these two elemental ratios can be the result of secondary aragonite or calcite precipitation (Quinn and Taylor, 2006; Sayani et al., 2011). *Siderastrea siderea* is a relatively slow-growing coral (~6 mm year^{-1}) when compared with other corals, yet its growth rate is more than sufficient to visually discern years in the density bands and for geochemical sampling on annual to weekly time scales. There is no distinct visible marker or litho-facies change for the year 1957 in the core 05WFGB3 but the year can be found by counting the annual density bands that are visible (wetting the surface helps to see the bands) but are easier to see in X-radiographs. Counting annual bands provides accurate dating and chronology control for corals similar to dendrochronology (Black et al., 2019). Furthermore, corals can be ^{230}Th-dated with accuracies better than ±1 year for corals <100 years old when a single annual density band is dated (Shen et al., 2003, 2008). WFGB is an open ocean location managed and protected by the FGBNMS that is accessible by boat and to divers. FGBNMS also coordinates and compiles all research conducted in FGB in annual and other reports (Johnston et al., 2021).

Geochemical proxies are the primary markers used for chemostratigraphy in a coral skeleton such that researchers can examine how their variations are influenced by the evolution of global

and regional anthropogenic activities (Figure 2). The fallout from atmospheric thermonuclear weapon testing is a significant, globally widespread, and abrupt signature that can be used as a global marker for the onset of human-dominated changes in the environment (Waters et al., 2015). However, the timing and amplitude of the bomb spikes in the surface ocean and thus corals can be affected by (1) location, (2) atmospheric distribution, (3) the rate of equilibration with the atmosphere, (4) the hydrographic regime of the location, (5) biological uptake of radioactive isotopes. The peak of thermonuclear testing occurred in 1951–1958 and 1961–1962 and declined after 1963 due to a Partial Test Ban Treaty and moratoriums when testing was mainly underground in the late 1960s (UNSCEAR, 2000).

Coral core 05WFGB3 contains the radiocarbon "bomb spike" with an increase starting in 1957 then a peak acceleration in 1962 and reaching a maximum in 1970 (Figure 2). Radiocarbon enters the ocean through gas exchange with the atmosphere with an equilibration time of 7–10 years (Broecker and Peng, 1982; Mahadevan, 2001). The bomb $\Delta^{14}C$ maximum in core 05WFGB3 exhibits this expected delay with respect to the atmosphere and the initial increase and acceleration is within the testing dates. The GoM corals do not contain the ^{14}C water mixing signal seen in the $\Delta^{14}C$ in corals from the Cariaco Basin and south of Puerto Rico from equatorial waters with ^{14}C depleted water (Figure 3) (Kilbourne et al., 2007; Wagner et al., 2009; Wagner, 2011). Previous GoM coral $\Delta^{14}C$ studies found the source waters that feed the GoM and the air-sea exchange of CO_2 in the gulf are close to the global average (Wagner et al., 2009, Wagner 2011). Therefore, the $\Delta^{14}C$ in core 05WFGB3 is representative of a more global radiocarbon bomb spike than locations with upwelling and mixing water masses that contain ^{14}C-depleted water or locations near the weapons testing sites.

Plutonium-239 is a significant component of the radioactive fallout from thermonuclear weapons testing with a half-life of 24,110 years that will be detectable for ~100,000 years (Hancock et al., 2014) whereas ^{14}C is detectable for ~55,000 years (Hajdas et al., 2021). The coral $^{239+240}Pu$ record has two clearly marked "bomb spikes" in 1956 and 1964. These spikes are synchronous (± 1–2 years) with other tropical Atlantic corals but occur after the bomb spikes in Pacific corals located closer to the testing sites (Sanchez-Cabeza et al., 2021) (Figures 2 and 4) suggesting the WFGB coral is recording wind distributed ^{239}Pu thus a more global bomb spike (Waters et al., 2018). Since the WFGB coral and Haiti microatoll coral are synchronous for the 1956 spike, this suggests water depth and oceans currents are not a factor for these coral $^{239+240}Pu$ records; however, there are differences in the magnitude of $^{239+240}Pu$ activities for the Atlantic corals (Figure 4) suggesting a possible biological effect that could be contributing to the coral $^{239+240}Pu$ activities. Another consideration when comparing the $\Delta^{14}C$ and $^{239+240}Pu$ records in core 05WFGB3 is analytical precision and detection limits where the plutonium analysis was not different from the background for several samples analyzed for this study (Supplemental Figure 8) whereas the $\Delta^{14}C$ spike is much greater than analytical precision. Other radioactive isotopes investigated in this study were not detectable in corals possibly due to oceanic or biological processes.

At the same time as nuclear testing was occurring, pollution from industry, fossil fuel burning, and other human activities was rapidly increasing and these proxies can serve as auxiliary Anthropocene markers. The decreasing trend since the 1800s in coral $\delta^{13}C$ due to fossil fuel burning has been studied in corals since 1978 (Swart et al., 2010). The decreasing trend in $\delta^{13}C$ is accelerating especially after the year 2000 and is almost in sync with atmospheric $\delta^{13}C$ due to the oceans up taking atmospheric CO_2 (Figure 5b) The $\delta^{13}C$ Suess effect is captured in many carbon-based archives that could also be used as chemostratigraphic tool. Parallel to the increasing fossil fuel burning is the addition of greenhouse gases in the atmosphere that is driving temperatures higher. The WFGB coral Sr/Ca is recording these temperature changes in the ocean (Figures 2 and 5b) and contains the global warming trend. However, the timing of the warming trend does vary by

location and is not globally synchronous to a year or even a decade (Abram et al., 2016; PAGES 2k Consortium, 2013) but could serve as marker in a wide array of archives with resolutions that are not always annual. Mercury levels in the environment have tripled since the pre-industrial interval with an increase after World War II (Horowitz et al., 2014). The WFGB coral Hg record captures this variability (Figure 2) and fluctuates with Hg consumption and production (Kelly and Matos, 2014) (Figure 7b). Oil extraction operations using barite as a drilling mud have increased seawater Ba concentration in the GoM (Carriquiry and Horta-Puga, 2010; Deslarzes et al., 1995; Weerabaddana et al., 2021). The increase in mean coral Ba/Ca after 1965 represents the increase in global oil and gas demand after World War II (Figure 2). The coral Ba/Ca record is an indicator of the onset of anthropogenic activities in the GoM yet its scope remains regional and precludes its uses as an Anthropocene marker.

The GoM is intimately linked to North America via the Mississippi River and other rivers that bring anthropogenic pollutants from land to the ocean (mercury and nitrogen). The CS-δ^{15}N record in core 05WFGB3 provides an invaluable perspective on the alteration of the marine nitrogen cycle in the GoM due to recent anthropogenic activities. A significant increase in CS-δ^{15}N is observed after 1963. Transforming forests to agricultural lands and grasslands in the era of "rapid acceleration" accompanied by the massive use of artificial fertilizer during the Green Revolution starting in the 1960s (Ruddiman et al., 2015) to meet the world's food supply needs has remarkably changed the ocean nitrogen cycle by the increased nutrient loading from agricultural systems. Exposed soil is prone to erosion and nutrient leaching that ended up in the oceans through river runoff is revealed in our coral record (Figures 2 and 6). Although this record is surely a robust indicator of the onset of the anthropogenic footprint on the GoM and North America, its scope remains regional and precludes its use as an Anthropocene marker.

Conclusions

Corals are a unique archive presented here as a candidate for the Anthropocene GSSP. Corals are simultaneously recording the changes that we humans are making to our planet while also on the verge of becoming extinct themselves. Predictions for corals and coral reefs are that they could be dead by 2030 CE in some locations and by 2100 CE for most reefs. Hopefully, a few corals in places of refugia may survive, such as Flower Garden Banks. As the scientific community debates the Anthropocene, the GSSP site, and the year for the start of the Anthropocene, corals will ultimately become the recorder of their last years, passively archiving the changes in their environment, chronologize their stressors, the pollutants, and damage done to these otherwise multi-centenarians living organisms that are now doomed by humans to become a part of the rock record and no longer a part of the living planet Earth.

students Gilman Ouellette, Jacob Warner, Deborah Loke, Ashley Pomes, Othalia Roberts, Kendall Brome, and lab coordinator Sarah Crabtree for their efforts during this project. Coral data associated with this article are provided in a Supplemental Excel file. The authors are not aware of any affiliations, memberships, funding, or financial holdings that might be perceived as affecting the objectivity of this research.

ORCID iDs

Kristine L DeLong [iD] https://orcid.org/0000-0001-6320-421X

Amy J Wagner [iD] https://orcid.org/0000-0002-1979-8919

Jonathan Jung [iD] https://orcid.org/0000-0002-2739-9926

Irka Hajdas [iD] https://orcid.org/0000-0003-2373-2725

Simon D Turner [iD] https://orcid.org/0000-0001-8692-8210

Jens Zinke [iD] https://orcid.org/0000-0002-0634-8281

Supplemental material

Supplemental material for this article is available online.

References

Abram NJ, McGregor HV, Tierney JE, et al. (2016) Early onset of industrial-era warming across the oceans and continents. *Nature* 536(7617): 411–418.

Alibert C, Kinsley L, Fallon SJ, et al. (2003) Source of trace element variability in Great Barrier Reef corals affected by the Burdekin flood plumes. *Geochimica et Cosmochimica Acta* 67(2): 231–246.

Allard J, Clarke Iii JV and Keim BD (2016) Spatial and temporal patterns of *In Situ* sea surface temperatures within the Gulf of Mexico from 1901-2010. *American Journal of Climate Change* 05: 314–343.

Alvera-Azcárate A, Barth A and Weisberg RH (2009) The surface circulation of the Caribbean Sea and the Gulf of Mexico as inferred from satellite altimetry. *Journal of Physical Oceanography* 39(3): 640–657.

Bastidas C and García E (2004) Sublethal effects of mercury and its distribution in the coral *Porites astreoides. Marine Ecology Progress Series* 267: 133–143.

Benninger LK and Dodge RE (1986) Fallout plutonium and natural radionuclides in annual bands of the coral *Montastrea annularis*, St. Croix, U.S. Virgin Islands. *Geochimica et Cosmochimica Acta* 50(12): 2785–2797.

Black BA, Andersson C, Butler PG, et al. (2019) The revolution of crossdating in marine palaeoecology and palaeoclimatology. *Biology Letters* 15(1): 20180665.

Bleiwas DI and Miller MM (2015) *Barite—A Case Study of Import Reliance on an Essential Material for Oil and Gas Exploration and Development Drilling*. Washington, DC: U.S. Geological Survey.

Broecker WS and Peng T-H (1982) *Tracers in the Sea*. Palisades, NY: Lamont-Doherty Geological Observatory, Columbia University.

Buddemeier RW, Maragos JE and Knutson DW (1974) Radiographic studies of reef coral exoskeletons: Rates and patterns of coral growth. *Journal of Experimental Marine Biology and Ecology* 14(2): 179–199.

Buesseler KO (1997) The isotopic signature of fallout plutonium in the North Pacific. *Journal of Environmental Radioactivity* 36(1): 69–83.

Carriquiry JD and Horta-Puga G (2010) The Ba/Ca record of corals from the southern Gulf of Mexico: Contributions from land-use changes, fluvial discharge and oil-drilling muds. *Marine Pollution Bulletin* 60(9): 1625–1630.

Cheng H, Lawrence Edwards R, Shen CC, et al. (2013) Improvements in ^{230}Th dating, ^{230}Th and ^{234}U half-life values, and U–Th isotopic measurements by multi-collector inductively coupled plasma mass spectrometry. *Earth and Planetary Science Letters* 371-372: 82–91.

Darnell RM and Defenbaugh RE (2015) Gulf of Mexico: Environmental overview and history of environmental research. *American Zoologist* 30(1): 3–6.

Dassié EP, Lemley GM and Linsley BK (2013) The Suess effect in Fiji coral δ^{13}C and its potential as a tracer of anthropogenic CO_2 uptake. *Palaeogeography Palaeoclimatology Palaeoecology* 370(0): 30–40.

David MB, Drinkwater LE and McIsaac GF (2010) Sources of nitrate yields in the Mississippi River basin. *Journal of Environmental Quality* 39(5): 1657–1667.

Dee SG, Torres MA, Martindale RC, et al. (2019) The future of reef ecosystems in the Gulf of Mexico: Insights from coupled climate model simulations and ancient hot-house reefs. *Frontiers in Marine Science* 6: 691.

DeLong KL, Flannery JA, Maupin CR, et al. (2011) A coral Sr/Ca calibration and replication study of two massive corals from the Gulf of Mexico. *Palaeogeography Palaeoclimatology Palaeoecology* 307(1–4): 117–128.

DeLong KL, Flannery JA, Poore RZ, et al. (2014) A reconstruction of sea surface temperature variability in the southeastern Gulf of Mexico from 1734 to 2008 C.E. using cross-dated Sr/Ca records from the coral *Siderastrea siderea. Paleoceanography* 29(5): 403–422.

DeLong KL, Maupin CR, Flannery JA, et al. (2016) Refining temperature reconstructions with the Atlantic coral *Siderastrea siderea. Palaeogeography Palaeoclimatology Palaeoecology* 462: 1–15.

DeLong KL, Quinn TM, Taylor FW, et al. (2013) Improving coral-base paleoclimate reconstructions by replicating 350 years of coral Sr/Ca variations. *Palaeogeography Palaeoclimatology Palaeoecology* 373: 6–24.

Deslarzes KJP, Boothe PN, Presley BJ, et al. (1995) Historical incorporation of barium in the reef building coral *Montastrea annularis* at the Flower Garden Banks, north-west Gulf of Mexico. *Marine Pollution Bulletin* 30(11): 718–722.

Duprey NN, Wang TX, Kim T, et al. (2020) Megacity development and the demise of coastal coral communities: Evidence from coral skeleton δ^{15}N records in the Pearl River estuary. *Global Change Biology* 26(3): 1338–1353.

Duprey NN, Wang XT, Thompson PD, et al. (2017) Life and death of a sewage treatment plant recorded in a coral skeleton δ^{15}N record. *Marine Pollution Bulletin* 120(1-2): 109–116.

Erler DV, Wang XT, Sigman DM, et al. (2015) Controls on the nitrogen isotopic composition of shallow water corals across a tropical reef flat transect. *Coral Reefs* 34(1): 329–338.

Flannery JA, Richey JN, Thirumalai K, et al. (2017) Multi-species coral Sr/Ca-based sea-surface temperature reconstruction using *Orbicella faveolata* and *Siderastrea siderea* from the Florida Straits. *Palaeogeography Palaeoclimatology Palaeoecology* 466: 100–109.

Frieler K, Meinshausen M, Golly A, et al. (2013) Limiting global warming to 2°C is unlikely to save most coral reefs. *Nature Climate Change* 3(2): 165–170.

Froehlich MB, Tims SG, Fallon SJ, et al. (2017) Nuclear weapons produced ^{236}U, ^{239}Pu and ^{240}Pu archived in a *Porites Lutea* coral from Enewetak Atoll. *Journal of Environmental Radioactivity 178-179*: 349–353.

Greene CA, Thirumalai K, Kearney KA, et al. (2019) The climate data toolbox for MATLAB. *Geochemistry Geophysics Geosystems* 20(7): 3774–3781.

Guzmán HM and García EM (2002) Mercury levels in coral reefs along the Caribbean coast of Central America. *Marine Pollution Bulletin* 44(12): 1415–1420.

Hajdas I, Ascough P, Garnett MH, et al. (2021) Radiocarbon dating. *Nature Reviews Methods Primers* 1(1): 62.

Hancock GJ, Tims SG, Fifield LK, et al. (2014) The release and persistence of radioactive Anthropogenic nuclides. *Geological Society of London*, *Special Publications* 395(1): 265–281.

Head MJ and Gibbard PL (2015) Formal subdivision of the Quaternary System/Period: Past, present, and future. *Quaternary International* 383: 4–35.

Horowitz HM, Jacob DJ, Amos HM, et al. (2014) Historical mercury releases from commercial products: Global environmental implications. *Environmental Science & Technology* 48(17): 10242–10250.

Johnston MA, Hickerson EL, Nuttall MF et al. (2019) Coral bleaching and recovery from 2016 to 2017 at East and West Flower Garden Banks, Gulf of Mexico. *Coral Reefs* 38(4): 787–799.

Johnston MA, O'Connell K, Blakeway RD, et al. (2021) *Long-Term Monitoring at East and West Flower Garden Banks: 2019 Annual Report. National Marine Sanctuaries Conservation Series ONMS-21-02*. Galveston, TX: U.S. Department of Commerce, National Oceanic and Atmospheric Administration, Flower Garden Banks National Marine Sanctuary.

Keeling CD (1979) The Suess effect: ^{13}Carbon-^{14}Carbon interrelations. *Environment International* 2(4–6): 229–300.

Keeling CD, Piper SC, Bacastow RB, et al. (2001) Exchanges of atmospheric CO_2 and $^{13}CO_2$ with the terrestrial biosphere and oceans from 1978 to 2000. I. Global aspects, SIO Reference Series, No. 01-06, Scripps Institution of Oceanography, San Diego.

Kelly TD and Matos GR (2014) *Historical Statistics for Mineral and Material Commodities in the United States (2016 version)*. Washington, DC: U.S. Geological Survey Data Series.

Kilbourne KH, Quinn TM, Guilderson TP, et al. (2007) Decadal- to interannual-scale source water variations in the Caribbean Sea recorded by Puerto Rican coral radiocarbon. *Climate Dynamics* 29(1): 51–62.

Killick R, Fearnhead P and Eckley IA (2012) Optimal detection of changepoints with a linear computational cost. *Journal of the American Statistical Association* 107(500): 1590–1598.

Knutson DW, Buddemeier RW and Smith SV (1972) Coral chronometers: Seasonal growth bands in reef corals. *Science* 177(4045): 270–272.

Kuffner IB, Roberts KE, Flannery JA, et al. (2017) Fidelity of the Sr/Ca proxy in recording ocean temperature in the western Atlantic coral *Siderastrea siderea. Geochemistry Geophysics Geosystems* 18(1): 178–188.

Lawman AE, Dee SG, DeLong KL, et al. (2022) Rates of future climate change in the Gulf of Mexico and the Caribbean Sea: Implications for Coral Reef Ecosystems. *Journal of Geophysical Research Biogeosciences* 127(9): e2022JG006999.

Lea DW, Shen GT and Boyle EA (1989) Coralline barium records temporal variability in equatorial Pacific upwelling. *Nature* 340(6232): 373–376.

Lindahl P, Andersen MB, Keith-Roach M, et al. (2012) Spatial and temporal distribution of Pu in the Northwest Pacific Ocean using modern coral archives. *Environment International* 40: 196–201.

Lindahl P, Asami R, Iryu Y, et al. (2011) Sources of plutonium to the tropical Northwest Pacific Ocean (1943–1999) identified using a natural coral archive. *Geochimica et Cosmochimica Acta* 75(5): 1346–1356.

Lough JM and Cantin NE (2014) Perspectives on massive coral growth rates in a changing ocean. *The Biological Bulletin* 226(3): 187–202.

Mahadevan A (2001) An analysis of bomb radiocarbon trends in the Pacific. *Marine Chemistry* 73(3–4): 273–290.

Murray SP, Jarosz E and Weeks ET III (1998) An observational study of the Mississippi- Atchafalaya coastal plume: Final report. U.S. Department of the Interior, Minerals Management Service, Gulf of Mexico OCS Region, New Orleans, LA.

Noshkin VE, Wong KM, Eagle RJ, et al. (1975) Transuranics and other radionuclides in Bikini Lagoon: Concentration data retrieved from aged coral sections. *Limnology and Oceanography* 20(5): 729–742.

Office of National Marine Sanctuaries (2008) *Flower Garden Banks National Marine Sanctuary Condition Report 2008*. Silver Spring, MD: U.S. Department of Commerce, National Oceanic and Atmospheric Administration, Office of National Marine Sanctuaries.

PAGES 2k Consortium (2013) Continental-scale temperature variability during the past two millennia. *Nature Geoscience* 6(5): 339–346.

Paillard D, Labeyrie L and Yiou P (1996) Macintosh program performs time-series analysis. *Eos Transactions American Geophysical Union* 77: 379–379.

Prouty NG, Goodkin NF, Jones R, et al. (2013) Environmental assessment of metal exposure to corals living in Castle Harbour, Bermuda. *Marine Chemistry* 154: 55–66.

Prouty NG, Roark EB, Koenig AE, et al. (2014) Deep-sea coral record of human impact on watershed quality in the Mississippi River Basin. *Global Biogeochemical Cycles* 28(1): 29–43.

Pulster EL, Gracia A, Armenteros M, et al. (2020) A first comprehensive baseline of hydrocarbon pollution in Gulf of Mexico fishes. *Scientific Reports* 10(1): 6437.

Purdy CB, Druffel ERM and Hugh D L (1989) Anomalous levels of ^{90}Sr and ^{239,240}Pu in Florida corals: Evidence of coastal processes. *Geochimica et Cosmochimica Acta* 53(6): 1401–1410.

Quinn TM and Taylor FW (2006) SST artifacts in coral proxy records produced by early marine diagenesis in a modern coral from Rabaul, Papua New Guinea. *Geophysical Research Letters* 33: L04601.

Rabalais NN, Turner RE and Wiseman WJ (2002) Gulf of Mexico hypoxia, a.k.a "The Dead Zone". *Annual Review of Ecology and Systematics* 33(1): 235–263.

Reimer PJ (2004) Discussion: Reporting and calibration of post-bomb ^{14}C Data. *Radiocarbon* 46(3): 1299–1304.

Reynolds RW, Rayner NA, Smith TM, et al. (2002) An improved in situ and satellite SST analysis for climate. *Journal of Climate* 15(13): 1609–1625.

Rosenbauer RJ, Swarzenski PW, Kendall C, et al. (2009) A carbon, nitrogen, and sulfur elemental and isotopic study in dated sediment cores from the Louisiana Shelf. *Geo-Marine Letters* 29(6): 415–429.

Ruddiman WF, Ellis EC, Kaplan JO, et al. (2015) Geology. Defining the epoch we live in. *Science* 348(6230): 38–39.

Sanchez-Cabeza J-A, Rico-Esenaro SD, Corcho-Alvarado JA, et al. (2021) Plutonium in coral archives: A good primary marker for an Anthropocene type section. *The Science of the Total Environment* 771: 145077.

Sayani HR, Cobb KM, Cohen AL, et al. (2011) Effects of diagenesis on paleoclimate reconstructions from modern and young fossil corals. *Geochimica et Cosmochimica Acta* 75(21): 6361–6373.

Schmahl GP, Hickerson EL and Precht WF (2008) Biology and Ecology of Coral Reefs and Coral Communities in the Flower Garden Banks Region, Northwestern Gulf of Mexico. In: Riegl BM and Dodge RE (eds) *Coral Reefs of the USA*. Dordrecht: Springer, pp.221–261.

Shen C-C, Cheng H, Edwards RL, et al. (2003) Measurement of attogram quantities of ^{231}Pa in dissolved and particulate fractions of seawater by isotope dilution thermal ionization mass spectroscopy. *Analytical Chemistry* 75(5): 1075–1079.

Shen C-C, Li KS, Sieh K, et al. (2008) Variation of initial ^{230}Th/^{232}Th and limits of high precision U–Th dating of shallow-water corals. *Geochimica et Cosmochimica Acta* 72(17): 4201–4223.

Shen C-C, Wu CC, Cheng H, et al. (2012) High-precision and high-resolution carbonate ^{230}Th dating by MC-ICP-MS with SEM protocols. *Geochimica et Cosmochimica Acta* 99(0): 71–86.

Slowey NC, Holcombe T, Betts MP, et al. (2008) Habitat Islands along the shelf edge of the Northwestern Gulf of Mexico. In: Ritchie KB and Keller BD (eds) *A Scientific Forum on the Gulf of Mexico: The Islands in the Stream Concept. Marine Sanctuaries Conservation Series NMSP-08-04*. Silver Spring, MD: U.S. Department of Commerce, National Oceanic and Atmospheric Administration, National Marine Sanctuary Program, pp.22–27.

Smith TM, Reynolds RW, Peterson TC, et al. (2008) Improvements to NOAA's historical merged land–ocean surface temperature analysis (1880–2006). *Journal of Climate* 21(10): 2283–2296.

Sturges W and Evans JC (1983) On the variability of the Loop Current in the Gulf of Mexico. *Journal of Marine Research* 41(4): 639–653.

Sun R, Hintelmann H, Liu Y, et al. (2016) Two centuries of coral skeletons from the northern South China Sea record mercury emissions from modern Chinese wars. *Environmental Science & Technology* 50(11): 5481–5488.

Swart PK, Greer L, Rosenheim BE, et al. (2010) The C-13 Suess effect in scleractinian corals mirror changes in the anthropogenic CO_2 inventory of the surface oceans. *Geophysical Research Letters* 37: L05604.

Teague WJ, Wijesekera HW, Jarosz E, et al. (2013) Current and hydrographic conditions at the East Flower Garden Bank in 2011. *Continental Shelf Research* 63: 43–58.

UNSCEAR (2000) *Sources and Effects of Ionizing Radiation, 2000 Report*. New York: United Nations.

Wagner AJ (2011) *Oxygen and Carbon Isotopes and Coral Growth in the Gulf of Mexico and Caribbean Sea as Environmental and Climate Indicators*. PhD Dissertation, Texas A&M University, College Station.

Wagner AJ, Guilderson TP, Slowey NC, et al. (2009) Pre-bomb surface water radiocarbon of the Gulf of Mexico and Caribbean as recorded in hermatypic corals. *Radiocarbon* 51(3): 947–954.

Wang XT, Cohen AL, Luu V, et al. (2018) Natural forcing of the North Atlantic nitrogen cycle in the Anthropocene. *Proc Natl Acad Sci USA* 115(42): 10606–10611.

Wang XT, Sigman DM, Cohen AL, et al. (2016) Influence of open ocean nitrogen supply on the skeletal δ^{15}N of modern shallow-water scleractinian corals. *Earth and Planetary Science Letters* 441: 125–132.

Waters CN, Turner SD, Zalasiewicz J, et al. (2023) Candidate sites and other reference sections for the Global boundary Stratotype Section and Point (GSSP) of the Anthropocene series. *The Anthropocene Review* 10(1): 3–24 (in this issue).

Waters CN, Syvitski JPM, Gałuszka A, et al. (2015) Can nuclear weapons fallout mark the beginning of the Anthropocene Epoch? *Bulletin of the Atomic Scientists* 71(3): 46–57.

Waters CN, Zalasiewicz J, Summerhayes C, et al. (2018) Global Boundary Stratotype Section and Point (GSSP) for the Anthropocene Series: Where and how to look for potential candidates. *Earth-Science Reviews* 178: 379–429.

Weerabaddana MM, DeLong KL, Wagner AJ, et al. (2021) Insights from barium variability in a *Siderastrea siderea* coral in the northwestern Gulf of Mexico. *Marine Pollution Bulletin* 173: 112930.

Wilson WD and Johns WE (1997) Velocity structure and transport in the Windward Islands Passages. *Deep Sea Research Part I Oceanographic Research Papers* 44(3): 487–520.

Zavala-Hidalgo J, Romero-Centeno R, Mateos-Jasso A, et al. (2014) The response of the Gulf of Mexico to wind and heat flux forcing: What has been learned in recent years? *Atmósfera* 27(3): 317–334.